Time Courses of Mammalian Cell Electropermeabilization Observed by Millisecond Imaging of Membrane Property Changes during the Pulse

Bruno Gabriel and Justin Teissié
Institut de Pharmacologie et de Biologie Structurale-Centre National de la Recherche Scientifique (UPR 9062), F-31062 Toulouse, France

ABSTRACT Time courses of electropermeabilization were analyzed during the electric field application using a rapid fluorescent imaging system. Exchanges of calcium ions through electropermeabilized membrane of Chinese hamster ovary cells were found to be asymmetrical. Entry of calcium ions during a millisecond pulse occurred on the anode-facing cell hemisphere. Entry through the region facing the cathode was observed only after the pulse. Leakage of intracellular calcium ions from electropermeabilized cell in low-calcium content medium was observed only from the anode-facing side. The exchanges during the pulse were mostly due to diffusion-driven processes, i.e., governed by the concentration gradient. Interaction of propidium iodide, a dye sensitive to the structural alteration of membrane, with cell membrane was asymmetrical during electropermeabilization. Localized enhancement of the dye fluorescence was observed during and after the pulsation on the cell surface. Specific staining of a limited anode-facing part of the membrane was observed as soon as the pulse was applied. The membrane fluorescence level increased during and immediately after the pulse whereas the geometry of the staining was unchanged. The membrane regions stained by propidium iodide were the same as those where calcium exchanges occurred. The fraction of the membrane on which structural alterations occurred was defined by the field strength. The density of defects was governed by the pulse duration. Electropermeabilization is a localized but asymmetrical process. The membrane defects are created unequally on the two cell sides during the pulse, implying a vectorial effect of the electric field on the membrane.

INTRODUCTION

For more than two decades, it has been known that the application of brief (micro- to millisecond) intense (hundreds of volts per centimeter) external electric field pulses on living cells (electropulsation) makes the membrane transiently permeable (electropermeabilization) (Neumann and Rosenheck, 1972). Strict control of electric field parameters allows electropermeabilization to be reversible (Kinosita and Tsong, 1978; Neumann et al., 1982) and cell viability not to be greatly affected (Andreason and Evans, 1988; Gabriel and Teissié, 1995). Electropulsation is now frequently used in cell biology to introduce exogenous active compounds such as drugs (electrochemotherapy) (Mir et al., 1996), antibodies (Verspohl et al., 1997), or nucleic acids (electromediated gene transfer) (Van Dinten et al., 1997; Delgadillo et al., 1997) into various types of cells extensively. Other basic properties of electropermeabilized cell membrane are its associated fusogenicity (electrofusion) (Ogura et al., 1994) and its competence for a spontaneous insertion of proteins having a membrane-spanning sequence (electroinsertion) (El Ouagari et al., 1995).

Despite the widespread use of electropulsation in biology, the physical and structural origins of membrane destabilization remain unknown (Tsong, 1991). A clear understanding of them is a thrilling challenge. The driving force involved in electropermeabilization is an increase in the transmembrane electric potential difference, which, when larger than a threshold value (nowadays estimated between 0.25 and 0.6 V) (Benz et al., 1979; Teissié and Tsong, 1981; Marszalek et al., 1990; Teissié and Rols, 1993; Gabriel and Teissié, 1997), triggers a change in the permeability properties of the membrane. The geometrical and temporal dependence of this electro-induced phenomenon was experimentally demonstrated in single cells by the use of transmembrane electric-potential-sensitive electrochromic probes (Gross et al., 1986; Kinosita et al., 1988) and environment-dependent dyes (Gabriel and Teissié, 1997). Electropermeabilization of living cells is affected by the resting transmembrane electric potential difference (Tekle et al., 1990; Gabriel and Teissié, 1997). Quantification of molecule exchange showed that the part of the cell surface globally affected by the electric treatment depended on the electric field strength (Schwister and Deuticke, 1985; Rols and Teissié, 1990; Gabriel and Teissié, 1997). The pulse-induced local perturbation of the membrane structure is in the microsecond time range (Hibino et al., 1993). Therefore, analysis of the electropermeabilization processes requires work at the membrane level on single cells, with high temporal and spatial resolution. Tekle et al. (1994) showed that a selective asymmetrical transport of fluorescence dyes was observed across the electropermeabilized membrane after the pulsation. The video system was limited by its time resolution (33 ms/image), and transport patterns were only observed more than 300 ms after the end of the electric pulse. As they concluded, no data were available to indicate whether such asymmetric transport was present at earlier

Received for publication 16 November 1998 and in final form 19 January 1999.

Address reprint requests to Dr. Justin Teissié, Institut de Pharmacologie et de Biologie Structurale du CNRS (UPR 9062), 118 route de Narbonne, F-31062 Toulouse cedex 4, France. Tel.: 33-561335880; Fax: 33-561335860; E-mail: gabriel@ipbs.fr and justin@ipbs.fr.

0006-3495/99/04/2158/08 $2.00

times or during the pulse. Individual calcium entry sites were detected in adherent neuroblastoma cells (Teruel and Meyer, 1997). Rapid events in electropermeabilization of erythrocyte membrane were analyzed by measurement of voltage-induced membrane conductance showing a two-step process (Kinosita and Tsong, 1979; Teissié and Tsong, 1980). Millisecond measurements of the electro-induced leakage during a millisecond electropermeabilization pulse were obtained by a global fluorometry approach using a single calcein-loaded ghost (Prausnitz et al., 1995). However, no data were supplied about any localized transport through electropermeabilized membrane regions.

In the present study, using an ultra-rapid intensifying video system (3.33 ms/image), we directly observed exchanges of calcium ions between the cytosol of a single cell and the extracellular medium and the interaction of propidium iodide (PI) with the electropermeabilized parts of mammalian cell membrane during and immediately after a millisecond electropermeabilizing direct current (dc) pulse.

MATERIALS AND METHODS

Materials

PI (molecular weight 668.4) and $CaCl_2$ were purchased from Sigma Chemical Co. (St. Louis, MO). Fluo-3 AM and Fluo-3 free acid were obtained from Molecular Probes (Eugene, OR). Chelex-100 chelating resin was obtained from Bio-Rad (Richmond, CA). Standard isoosmotic pulsing buffer (PB) was 250 mM sucrose, 1 mM $MgCl_2$, and 10 mM potassium phosphate buffer (pH 7.4). Conductivity and osmotic pressure of PB were 1.5 mS/cm and 310 mOs/kg, respectively. Removal of calcium ions from PB and measurement of free calcium concentration of the solution were performed as previously described (Gabriel and Teissié, 1994).

Cell culture and labeling

Chinese hamster ovary (CHO) cells (WTT clone) were grown in suspension in Eagle's minimal essential medium (MEM 0111, Eurobio, Les Ulis, France) to avoid trypsin treatment, as previously described (Gabriel and Teissié, 1995). HeLa cells in suspension (S3 clone) were generously provided by C. Ramos (our institute). Cytosolic free calcium ion concentration was 220 ± 20 nM for CHO cells in suspension, and the free calcium ion concentration in PB was 2–4 μM (Gabriel and Teissié, 1994). The cell-permeant Fluo-3 AM (2.2 μM) was loaded (in the presence of 0.2% w/v F-127 pluronic acid) by incubating cells for 15–20 min in culture medium at room temperature and under gentle agitation. Excess external dye was washed off after incubation, and cells were suspended in 1 mM $CaCl_2$-containing PB. When external Ca^{2+} ions enter the electropermeabilized cell, they immediately bind to pre-loaded Fluo-3 indicators inside the cell and cause enhancement of fluorescence. For observation of the calcium efflux, we pulsed the cells in 100 nM calcium-containing PB in the presence of 10 μM Fluo-3 free acid indicator. When intracellular calcium ions (220 ± 20 nM) exit from the cell suspended in 100 nM calcium-containing PB they immediately bind to Fluo-3 indicator outside the cell and give an enhancement in fluorescence.

Cell electropermeabilization

Cells were harvested by centrifugation for 10 min at 100 × *g* (700 rpm, C500 centrifuge, Jouan, St. Herblain, France), washed with PB, and resuspended in PB containing the appropriate dye (PI or Fluo-3; 10^6 cells/ml). Propidium is a small positively charged ($z = 2$) phenanthrene derivative that is naturally relatively membrane impermeant and that has a spectrum and quantum yield that are environment dependent. It was classically used to quantify long-lived cell electropermeabilization. When the dye enters the electropermeabilized cell it binds to intracellular targets (DNA and/or RNA) and its fluorescence strongly increases. We previously showed that PI was an efficient tool for the study of electro-induced membrane alterations because of its change in fluorescence when bound to membrane loci (Gabriel and Teissié, 1997). The PS10 CNRS electropulser (Jouan) was used to supply a single square-wave electric pulse. Pulse parameters (voltage and duration) were monitored through a 15-MHz oscilloscope (Enertec, St. Etienne, France). The electropulsation chamber was made by using two stainless steel parallel rods (diameter 0.5 mm, length 10 mm, inter-electrode distance 5 mm) stuck on a glass microscope coverslip. The chamber was placed on the stage of an inverted digitized video-microscope as previously described (Gabriel and Teissié, 1997). A 70-μl cell suspension volume was poured between the electrodes. The electric pulse was applied, and fluorescence images of the electropulsed cell were recorded synchronously. For single CHO or HeLa cell observation data dealing with time courses of PI interaction with the cell are reported for those cells with an average radius equal to 6.5 μm.

Fluorescence image acquisition and processing

The ultra-rapid fluorescence image acquisition system and its synchronization with pulse delivery were previously described (Gabriel and Teissié, 1998). CHO cells were observed by fluorescence under the 63 × 1.4 NA oil immersion objective (Leitz, Wetzlar, Germany). When PI was used, the wavelengths were selected with a Leitz N2 block filter (530 nm $\leq \lambda_{exc} \leq$ 560 nm; 580 nm $\leq \lambda_{em}$). For Fluo-3 pre-loaded cells, the Leitz H3 filter block was used (390 nm $\leq \lambda_{exc} \leq$ 490 nm; 515 nm $\leq \lambda_{em}$). The LH 750-ULL camera (Lhesa, Cergy-Pontoise, France) allowed real-time fluorescence image acquisition with a 300-Hz frequency (3.33 ms/image). The size of the pixel was 0.3 × 0.2 μm. The fluorescence patterns of the dye during and after electropulsation of the cell were recorded in the memory board of the camera control box. The system allowed the acquisition of a single 20-ms video frame that represented six consecutive 3.33-ms images. The first one was acquired immediately before the onset of the pulse (blank image, i.e., the fluorescence image of the selected cell before electropulsation).

The recorded images were transferred to a PC computer (AT/486) by using a frame-grabber board (IP8, Matrox, Québec, Canada). The video signal was converted to a numerical matrix with 8-bit gray scale, i.e., 256 different light levels. The gain of the camera was fixed by manual adjustment. Image acquisition and processing were obtained with Optimas 4.02 software (Bioscan, Edmonds, WA) as previously described (Gabriel and Teissié, 1998). Images were corrected for the background; i.e., the blank image was subtracted from the fluorescence images of the cell recorded during and after the pulse. Geometry of the cell labeling was defined by digitized image processing (UTHSCSA ImageTool program, available by anonymous FTP from maxrad6.uthscsa.edu). Labeled areas of cells were bordered on the binary image created by manual thresholding of the gray-scale image (Macro-command: *threshold*). The polar angle associated with the labeled cap was measured by determining the angle defined by three points within the digital image (Macro-command: *angle*). Fluorescence emission of the labeled parts of cells was quantified by measurement of the gray level at a given time t after the rising edge of the pulse ($F(t)$) for the region of interest we had previously selected. One-dimensional light level distributions were obtained using Microsoft Excel 7.0a (Microsoft Corp., Redmond, WA). Final images were prepared for printing with Paint Shop Pro 3.11 software (JACS, Minnetonka, MN). We used the printer driver software XLI Bitmap SuperDriver (XLI Corp., Woburn, MA) for the HP laserjet 4 printer (Hewlett Packard, Camas, WA) to obtain high-resolution halftone prints (2400 dpi).

RESULTS

Electropermeabilization of mammalian cells in suspension was monitored by imaging electro-induced calcium ion exchanges and PI fluorescence changes.

Time course of Ca^{2+} influx into single electropermeabilized CHO cells

Fig. 1 shows the typical sequences of images synchronously obtained with the application of a single pulse of 1.0 kV/cm with 3- and 6-ms durations, on a Fluo-3 pre-loaded CHO cell in 1 mM Ca^{2+}-containing PB. The data show that during the pulse Ca^{2+} ions enter the cell exclusively through the side facing the anode. An increase of fluorescence was associated with the influx of external Ca^{2+} ions and began during the first 3.33 ms of the electropermeabilization pulse. Ca^{2+} ions kept on entering when the electric field was switched off as shown by the fluorescence expansion inside the anode-facing cell hemisphere with time (Fig. 1). A 1.0-kV/cm pulse is known to promote permeabilization of the two CHO cell sides (Gabriel and Teissié, 1997). Ca^{2+} ions enter the cell through the membrane facing the cathode but only when the field is switched off (Fig. 1). As observed for the anode-facing side, fluorescence then spreads inside the cathode-facing cell hemisphere area with time. Fig. 2 shows the one-dimensional fluorescence level profiles along the pole-to-pole axis of electropermeabilized cells in 1 mM Ca^{2+}-containing PB. Calcium spreading associated with the entry of external calcium through both cell sides was observed in the cell after electropermeabilization. The intracellular calcium concentration strongly increased locally on the anode-facing cell hemisphere and became saturating for the Fluo-3 indicator (Kd = 450 nM).

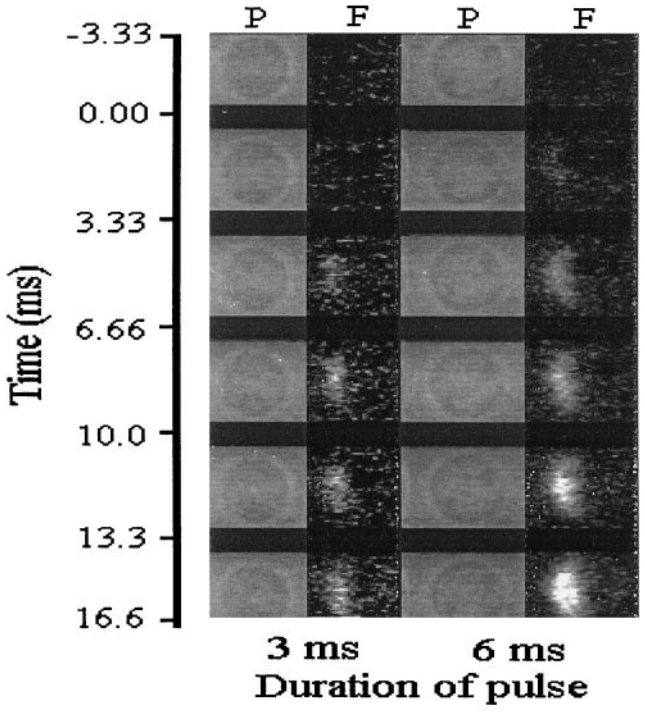

FIGURE 1 Typical time courses of calcium ion transport across electropermeabilized membrane of a single CHO cell. P, phase-contrast images; F mathematically processed fluorescence images (i.e., raw unprocessed fluorescence images obtained synchronously with pulsation minus those obtained before pulsation) (Gabriel and Teissié, 1998). CHO cells were previously loaded with Fluo-3 calcium indicator. Electropermeabilization was achieved in 1 mM $CaCl_2$-containing PB. Electric conditions were one square wave dc pulse of 1.0 kV/cm with various durations (3 and 6 ms). The position of the electrodes is positive (anode) to the left and negative (cathode) to the right of the frame. Image acquisition frequency was 300 Hz (3.33 ms/image). The localized increased peripheral fluorescence areas indicate the entry sites of extracellular calcium across the membrane.

Time course of Ca^{2+} efflux from single electropermeabilized CHO cells

Application of one single 10-ms pulse to a CHO cell in 100 nM Ca^{2+}, 10 μM Fluo3-containing PB led to a cloud of fluorescence appearing outside the cell during the pulse only when the electric field strength was higher than an apparent threshold (~0.7 kV/cm) (Fig. 3 *A*). The fluorescence cloud was still observed after the end of the pulse. This reflected efflux of intracellular free calcium ions from

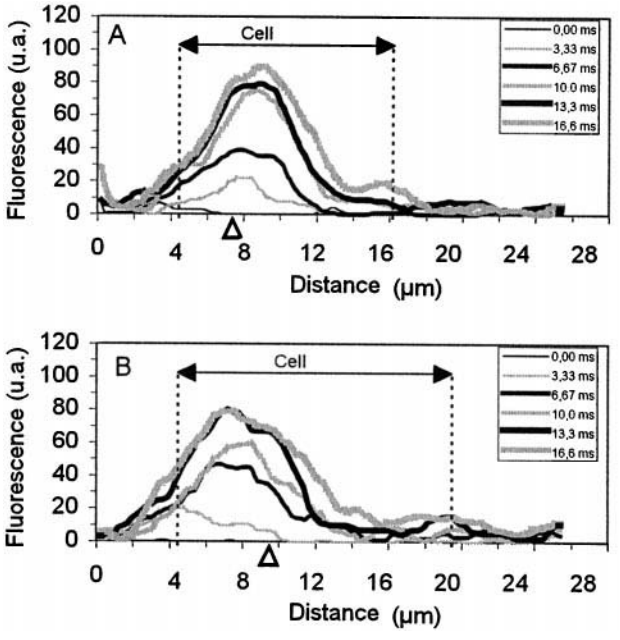

FIGURE 2 Cytosolic calcium spreading associated with the entry of exogenous calcium ions. One-dimensional distribution of the fluorescence levels associated with pixels along the cell axis parallel to the external field (pole-to-pole line) are presented for different times when the cell was pulsed using one single 1.0-kV/cm pulse of (*A*) 3 ms and (*B*) 6 ms. Data were from 3.33-ms images as in Fig. 1. Time 0.00 ms is representative of the one-dimensional profile observed just before electric field application. The other times represent the time lag after the beginning of the pulse application. Bars indicate the cell body. Open arrows indicate the projection of the cap border point on the *x* axis, as defined by the characteristic angle θ^{a}_{exp} when pulsing cells with one single 1.0-kV/cm pulse (63° and 69° for a 6-μm and 8-μm cell, respectively).

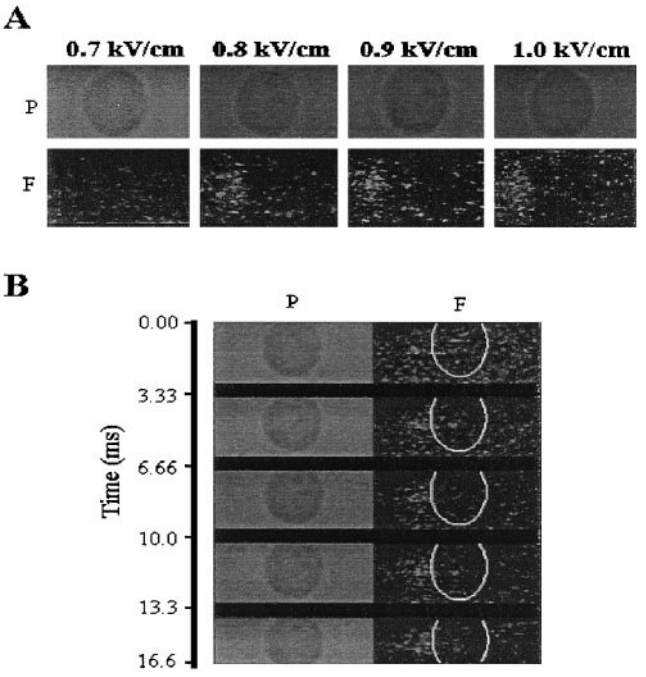

FIGURE 3 Calcium ion efflux associated with CHO cell membrane electropermeabilization. Electropermeabilization was achieved in 100 nM $CaCl_2$-containing PB, in the presence of 10 μM extracellular Fluo-3 free acid. The position of the electrodes, acquisition frequency, and image processing are as in Fig. 2. P, phase-contrast images; F, mathematically processed fluorescence images. (*A*) Selected video frames showing the calcium ion efflux associated with electropulsed cells. CHO cells were electropulsed using one 10-ms pulse with increasing field strength. The extracellular peripheral fluorescence cloud indicates the exit side of intracellular free calcium across the membrane.(*B*) Time course of calcium ion efflux across electropermeabilized membrane of single CHO cell. The pre-pulse image was subtracted from each in- and post-pulse image. Electric conditions were one 10-ms pulse of 1.0 kV/cm.

the cell through the positive electrode-facing hemisphere. A 0.9-kV/cm pulse is known to promote permeabilization of the two CHO cell sides (Gabriel and Teissié, 1997). However, we did not detect any efflux of calcium ions through the negative electrode-facing cell hemisphere within the observation time, i.e., up to 6 ms after the end of the pulse (Fig. 3 *B*).

Time course of PI interaction with single electropermeabilized CHO cells

Fig. 4 *A* shows the typical sequences of images obtained on a single CHO cell submitted to one pulse of 1.2 kV/cm with various durations (1.2 to 10 ms) in 1 mM PI-containing PB. Fig. 4 *B* shows the sequence obtained with HeLa cells. Similar results were obtained with the two cell types. Appearance of fluorescence enhancement was observed on the first image when the electric field was switched on. Interaction of PI with the cell membrane was visualized during the pulse by the localized area with enhanced fluorescence as previously observed after electropulsation (Gabriel and Teissié, 1997). The fluorescence areas during the pulse always faced the anode. We never observed peripheral fluorescence on the area facing the cathode in the time range of sequence acquisition. For 1.2 kV/cm, the geometry of the labeled area did not depend on the duration of the pulse (Fig. 4). The characteristic angle $\theta^a_{exp}(E)$ (the half of the polar angle associated with the labeled cap (Gabriel and Teissié, 1997)) was similar for CHO and HeLa cells (69° ± 3°, average cell radius of 6.5 μm). The dimension of the labeled part of the cell did not depend on PI concentration (data not shown) as previously reported (Tekle et al., 1994). The initial slope $(\Delta F/\Delta t)_i$ depended on the concentration of the dye when CHO cells in suspension were electropermeabilized with one single 3-ms pulse of 1.2 kV/cm, as expected (data not shown).

Dependence of PI interaction with electropermeabilized cell on the electric parameters

Anode-facing peripheral labeling observed during electropulsation was detected only when cells were treated with an electric field higher than an apparent threshold value of ~500 V/cm (data not shown). Above this apparent threshold value, an increase in electric field strength led to an increase in the dimension of the peripheral labeled cap present on the anode side of the cell as previously observed using ethidium bromide (Gabriel and Teissié, 1998). The characteristic angle $\theta^a_{exp}(E)$ depended on the electric field intensity (data not shown). A linear relationship was observed between $\cos(\theta^a_{exp}(E))$ and the reciprocal of the electric field intensity ($1/E$), which is related to the part of the cell membrane area that is globally electrically affected (Schwister and Deuticke, 1985; Rols and Teissié, 1990; Gabriel and Teissié, 1997). Extrapolation for $\cos(\theta^a_{exp}(E)) = 1$ allowed determination of the real threshold value of field strength inducing electropermeabilization ($E_p = 530 \pm 15$ V/cm).

The gray levels of the fluorescence regions ($F(t)$) were measured, and the kinetics of their increase were reported both for CHO and HeLa cells, when a single electropermeabilization pulse of 1.2 kV/cm with various durations was applied (Fig. 5). The fluorescence level increased linearly during the electropulsation and carried on to increase for some milliseconds when the electric field was switched off. For short pulse durations (1.2 and 3 ms), a plateau value was reached during the observation time (less than 16 ms). A steady state of alteration was then present. The fluorescent levels associated with this steady state were close to what was measured in a 40-ms time range after pulsation (data not shown; Gabriel and Teissié, 1997). For durations of pulse higher than 5 ms, the steady state of alteration was not reached during the observation time; fluorescence kept increasing. For a given electric field intensity, the initial slope $(\Delta F/\Delta t)_i$ of the electro-induced increase in fluorescence did not depend on the duration of the pulse. We obtained 9.92 ± 0.85 arbitrary unit/ms when a single pulse of 1.2 kV/cm was applied to the cell.

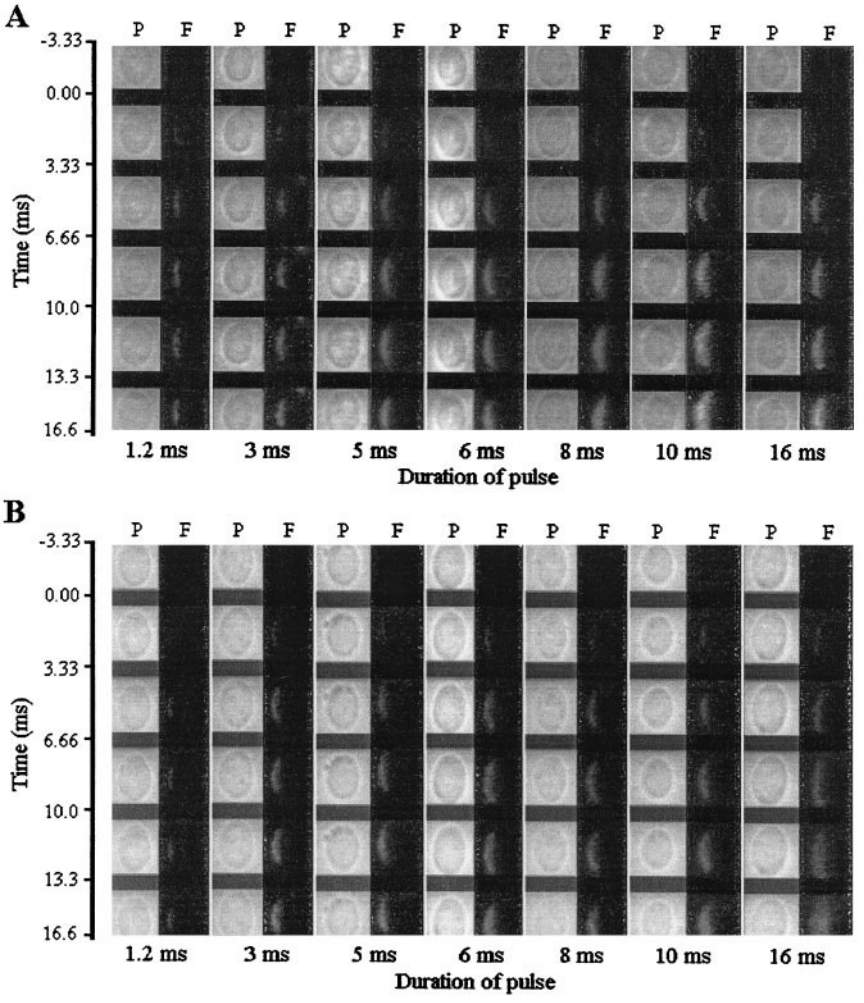

FIGURE 4 Time course of calcium PI interaction with electropermeabilized membrane of single (*A*) CHO cell and (*B*) HeLa cell. P, phase-contrast images; F, fluorescence images. Cells were electropermeabilized in 1 mM PI-containing PB, using one single pulse of 1.2 kV/cm with increasing duration. The position of the electrodes, acquisition frequency, and image processing are as in Fig. 2. The localized enhanced peripheral fluorescence indicates the PI-associated membrane staining. Zero on the time scale indicates the beginning of the electric pulse.

An increase in electric field strength led to an apparent increase in $(\Delta F/\Delta t)_i$ (Fig. 6 *A*). CHO cells in suspension were electropulsed by a single 3-ms pulse, in 1 mM PI-containing PB. A steady-state level of PI staining was reached ~6 ms after the end of the pulse whatever its electric intensity. The dependence of $(\Delta F/\Delta t)_i$ on the electric field intensity appeared as a linear function of $(1 - E_p/E)$ (data not shown), which directly represents the extent of the electropermeabilized membrane area (Rols and Teissié, 1990). We defined the surface fluorescence density (⟨fluorescence⟩) for a given electric field strength as $[F(t)/(1 - E_p/E)]$. Fig. 6 *B* shows the kinetics of the increase of ⟨fluorescence⟩ (⟨*F*⟩) we obtained using one 3-ms pulse with various electric field strengths. The initial slope $(\Delta\langle F\rangle/\Delta t)_i$ and the plateau value of the different curves did not depend on the electric field strength.

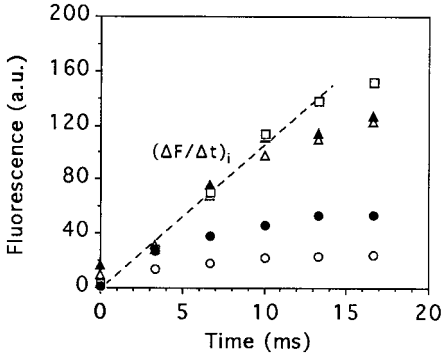

FIGURE 5 Dependence of the kinetics of PI-associated membrane staining on the duration of the pulse. CHO cells were electropermeabilized using one single pulse of 1.2 kV/cm, in 1 mM PI-containing PB. Durations of the pulse were as follows: ○, 1.2 ms; ●, 3 ms; △, 5 ms; ▲, 6 ms; □, 10 ms. $(\Delta F/\Delta t)_i$ is defined in the text. Data were from 3.33-ms images as in Fig. 4.

DISCUSSION

Effects of exogenous electric field on living cells are classically assessed via changes in two membrane parameters: transmembrane electrical potential difference and membrane permeability. Changes in transmembrane electrical potential difference have previously been monitored directly using the patch-clamp technique (Chernomordik et al., 1987; Tovar and Tung, 1992) and electrochromic dyes associated with video-microscopy (Gross et al., 1986; Kinosita et al., 1988). Membrane permeability changes have

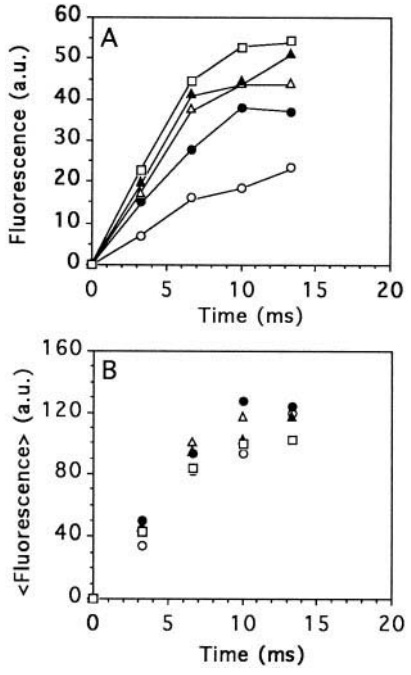

FIGURE 6 Effect of the electric field strength on the initial rate of PI-associated membrane staining appearance. CHO cells were pulsed in 1 mM PI-containing PB using one 3 ms-pulse. (*A*) Dependence of the initial rate $(\Delta F/\Delta t)_i$ on the electric field strength. Electric intensities were as follows: ○, 700 V/cm; ●, 800 V/cm; △, 900 V/cm; ▲, 1000 V/cm; □, 1200 V/cm. (*B*) Dependence of the kinetics of ⟨fluorescence⟩ increase on the electric field strength; ⟨fluorescence⟩ is defined as $[F(t)/(1 - E_p/E)]$ with E_p equal to 515 V/cm. Symbols are as above.

been monitored either by membrane conductance (Kinosita and Tsong, 1978; Hibino et al., 1991, 1993), or by analysis of efflux of molecule through the membrane (Rossignol et al., 1983; Mehrle et al., 1985; Dimitrov and Sowers, 1990; Kinosita et al., 1991; Tekle et al., 1990, 1994; Prausnitz et al., 1995; Djuzenova et al., 1996). Our approach allowed us to differentiate the behavior of the different parts of the cell surface.

When using electrical conditions that triggered permeabilization on the two cell sides, the behavior of the two electropermeabilized cell sides was different during the electric pulse. Ion exchange during the pulsation was observed only across the anode-facing side, i.e., the hyperpolarized one, but only after the pulse through the cathode-facing side (Fig. 1). Our observations agreed with those previously reported (Kinosita et al., 1991) with sea urchin eggs. In this case, the asymmetry in calcium exchanges was tentatively explained by a difference in the resealing kinetics of the two cell sides (Hibino et al., 1993). When the electric field was switched off, Ca^{2+} entry was still present. Our results could not be explained by electrophoretic drift induced by the externally applied electric field, giving a movement of Ca^{2+} ions from the cathode to the anode. Indeed, if the calcium concentration gradient through the plasma membrane (i.e., between the cell cytosol and extracellular medium) was inverted by using sub-cytosolic calcium content PB (100 nM), an efflux of calcium ions was observed during the pulse, but only through the anode-facing cell side (Fig. 3 *B*) as for the pulse-associated entry. Because the burst in fluorescence on the anode-facing cell side was observed only when the electric field intensity was higher than a threshold (0.7 kV/cm; Fig. 3 *A*), it could not be explained by a pulse-induced accumulation of extracellular calcium ions at the membrane/solution interface. The direction of this positive ion leakage was opposite to electric forces associated with electropulsation. Our findings are in apparent conflict with the involvement of electrophoretic transport during the pulse, as proposed by others (Dimitrov and Sowers, 1990; Prausnitz et al., 1995). Transport of calcium ions across the electropermeabilized membrane areas during the pulsation was mostly driven by the initial concentration gradient through the native membrane. It should be pointed out that in all our experiments on calcium transport, exchange of the calcium indicators between the permeabilized cell and the extracellular medium was not observed as previously reported (Tekle et al., 1994). The asymmetrical in-pulse transport could be explained by a difference in structures supporting electropermeabilization on the two cell sides as previously proposed (Teruel and Meyer, 1997). Membrane asymmetry between the two leaflets of the plasma membrane could explain the asymmetry of transport observed during the pulse (Teruel and Meyer, 1997). But from our results, we observed that when the pulse was switched off, transient permeation structures were detected on the two cell sides. In our work with spherical suspended cells, an electric field pulse induced a uniform calcium entry across the local electropermeabilized membrane area, although a small number of local calcium entry sites were previously reported using Fluo-3-pre-loaded adherent rat basophilic and neocortical neuroblastoma cells, which have highly irregular shapes (Teruel and Meyer, 1997). Again these previous results were consistent with a passive diffusion process (no contribution of electrophoresis or electroosmosis). The calcium influx associated with the cell electropermeabilization initiated an intracellular calcium spreading (Fig. 2).

We previously showed that interaction of PI with electropermeabilized CHO cells allowed direct visualization of the electropermeabilized parts of the cell membrane (Gabriel and Teissié, 1997). Similar interaction was observed using another cell type (Hela cell; Fig. 4 *B*). The threshold value for electropermeabilization of the anode cell side of the CHO cell was found to be 530 ± 15 V/cm. This value was similar to those generally reported. The same threshold was obtained for HeLa cells. Fluorescence of PI is highly environment dependent. It was previously described as a tool for the study of membrane structure because of its change in fluorescence when bound to membrane loci (Sator et al., 1977; Gabriel and Teissié, 1998). The increase in fluorescence quantum yield on binding to membrane reflects the immersion of the dye in a more structured and/or hydrophobic environment. Our data reported membrane staining by the dye on the anode-facing electropermeabi-

lized part of the cell specifically during the pulse, as previously proposed (Gabriel and Teissié, 1997, 1998). The increase of fluorescence observed during pulsation was not due to the binding of PI to its cytosolic targets after its transport through the membrane because a continuous increase of fluorescence intensity would be expected in this case as previously described (Sixou and Teissié, 1993). In our experiments, a steady-state level of fluorescence was reached (Fig. 5). In this study, we did not observe any labeling of the cathode-facing side of the cell whatever the field intensity in a 15-ms time lag after the end of the pulsation (Fig. 4). This suggested that the transient permeation structures present on this cell side behaved in a different way to those present on the anode-facing side.

Post-pulsation data showed that the fraction of the cell membrane globally affected depends on the electric field strength, and the extent of permeability depends on the duration of the pulse (Schwister and Deuticke, 1985; Rols and Teissié, 1990; Gabriel and Teissié, 1997). Figs. 4 and 5 illustrated that during the pulse, permeabilization affects a limited part of the cell surface. The dimension of the permeabilized anode-facing region was defined by the electric field intensity. Kinetics of membrane change during and after electropulsation were studied by analysis of time course of PI-associated membrane staining observed on the anode-facing hemisphere specifically. The kinetics were assessed using the initial rate $[(\Delta F/\Delta t)_i]$ of the increase of the fluorescence level of the stained region ($F(t)$). $F(t)$ macroscopically depicted the interaction of PI with the electro-induced new membrane sites. The steady-state level of membrane staining reached for short pulses depicted the final density of PI-stained sites. $(\Delta F/\Delta t)_i$ increased with the field strength (Fig. 6 *A*) because the number of PI interaction sites linearly increased with the membrane surface affected by the electrical treatment (defined by the electric intensity). $(\Delta\langle F\rangle/\Delta t)_i$ did not depend on the electric field strength (Fig. 6 *B*), showing that for a given pulse duration, the density of the electro-induced PI interaction sites, which was constant in the permeabilized cell cap, was the same whatever the applied field intensity. The alteration of the electropermeabilized membrane part was homogeneous. The surface density of the electro-induced sites depends only on the pulse duration.

For the first time, use of an ultra-rapid video system allowed us to directly observe, on single CHO cells, transport of free calcium ions through the electropermeabilized regions on the cell membrane surface, during and immediately after the pulsation. Differences in membrane alterations during and after the permeabilization pulse application were analyzed by associated changes in membrane staining by PI, in the millisecond time range. Our results show that the kinetics of membrane alteration that support electropermeabilization of mammalian cell membrane are different on the two electrode-facing sides during the pulse application. Electro-induced calcium ion flux through electropermeabilized membrane clearly demonstrated that a free diffusion process supported the transfer across the membrane and not only an electrophoretic one.

We thank Ms. C. Ramos for generous Hela cell supply, Mrs. C. Millot for CHO cell culture, Dr. P. Demange for his comments, and Mr. J. Robb for re-reading the manuscript.

This work was partly supported by a grant from the Association pour la Recherche contre le Cancer.

REFERENCES

Andreason, G. L., and G. A. Evans. 1988. Introduction and expression of DNA molecules in eukaryotic cells by electroporation. *BioTechniques*. 6:650–660.

Benz, R., F. Beckers, and U. Zimmermann. 1979. Reversible electrical breakdown of lipid bilayer membranes: a charge-pulse relaxation study. *J. Membr. Biol.* 48:181–204.

Chernomordik, L. V., S. I. Sukharev, S. V. Popov, V. F. Pastushenko, A. V. Sokirko, I. G. Abidor, and Y. A. Chizmadzhev. 1987. The electrical breakdown of cell and lipid membranes: the similarity of phenomenologies. *Biochim. Biophys. Acta*. 902:360–373.

Delgadillo, M. G., D. R. Liston, K. Niazi, and P. J. Johnson. 1997. Transient and selectable transformation of the parasitic protist *Trichomonas vaginalis*. *Proc. Natl. Acad. Sci. U.S.A.* 94:4716–4720.

Dimitrov, D. S., and A. E. Sowers. 1990. Membrane electroporation: fast molecular exchange by electroosmosis. *Biochim. Biophys. Acta*. 1022: 381–392.

Djuzenova, C. S., U. Zimmermann, H. Frank, V. L. Sukhorukov, E. Richter, and G. Fuhr. 1996. Effect of medium conductivity and composition on the uptake of propidium iodide into electropermeabilized myeloma cells. *Biochim. Biophys. Acta*. 1284:143–152.

El Ouagari, K., J. Teissié, and H. Benoist. 1995. Glycophorin A protects K562 cells from natural killer cell attack: role of oligosaccharides. *J. Biol. Chem.* 270:26970–26975.

Gabriel, B. and J. Teissié. 1994. Generation of reactive-oxygen species induced by electropermeabilization of Chinese hamster ovary cells and their consequence on cell viability. *Eur. J. Biochem.* 223:25–33.

Gabriel, B., and J. Teissié. 1995. Control by electrical parameters of short- and long-term cell death resulting from electropermeabilization of Chinese hamster ovary cells. *Biochim. Biophys. Acta*. 1266:171–178.

Gabriel, B., and J. Teissié. 1997. Direct observation in the millisecond time range of fluorescent molecule asymmetrical interaction with the electropermeabilized cell membrane. *Biophys. J.* 73:2630–2637.

Gabriel, B., and J. Teissié. 1998. Fluorescence imaging in the millisecond time range of membrane electropermeabilization of single cells using a rapid ultra-low-light intensifying detection system. *Eur. Biophys. J.* 27:291–298.

Gross, D., L. M. Loew, and W. W. Webb. 1986. Optical imaging of cell membrane potential changes induced by applied electric fields. *Biophys. J.* 50:339–348.

Hibino, M., H. Itoh, and K. Kinosita Jr. 1993. Time courses of cell electroporation as revealed by submicrosecond imaging of transmembrane potential. *Biophys. J.* 64:1789–1800.

Hibino, M., H. Sighemori, H. Itoh, K. Nagayama, and K. Kinosita. 1991. Membrane conductance of an electroporated cell analyzed by submicrosecond imaging of transmembrane potential. *Biophys. J.* 53:209–220.

Kinosita, K. Jr., and T. Y. Tsong. 1978. Voltage induced pore formation and hemolysis of human erythrocytes. *Nature*. 272:258–260.

Kinosita, K. Jr., and T. Y. Tsong. 1979. Voltage-induced conductance in human erythrocyte membranes. *Biochim. Biophys. Acta*. 554:479–497.

Kinosita, K. Jr., I. Ashikawa, N. Saita, H. Yoshimura, H. Itoh, K. Nagayama, and A. Ikegami. 1988. Electroporation of cell membrane visualized under a pulsed-laser fluorescence microscope. *Biophys. J.* 53: 1015–1019.

Kinosita, K. Jr., H. Itoh, S. Ishiwata, K. Hirano, T. Nishizaka, and T. Hayakawa. 1991. Dual-view microscopy with a single camera: real-time imaging of molecular orientation and calcium. *J. Cell Biol*. 115:67–73.

Marszalek, P., D. S. Liu, and T. Y. Tsong. 1990. Schwan equation and transmembrane potential induced by alternating electric field. *Biophys. J.* 58:1053–1058.

Mehrle, W., U. Zimmermann, and R. Hampp. 1985. Evidence for asymmetrical uptake of fluorescent dyes through electro-permeabilized membrane of *Avena* mesophyll protoplast. *FEBS Lett.* 185:89–94.

Mir, L. M., O. Tounekti, and S. Orlowski. 1996. Bleomycin: revival of an old drug. *Gen. Pharmacol.* 27:745–748

Neumann, E ., M. Schäfer-Ridder, Y. Yang, and P. D. Hofschneider. 1982. Gene transfer into mouse lyoma cells by electroporation in high electric fields. *EMBO J.* 1:841–845.

Neumann, E., and K. Rosenheck. 1972. Permeability changes induced by electric impulses in vesicular membranes. *J. Membr. Biol.* 10:279–290.

Ogura, A., J. Matsuda, and R. Yanagimachi. 1994. Birth of normal young after electrofusion of mouse oocytes with round spermatids. *Proc. Natl. Acad. Sci. U.S.A.* 94:7460–7462.

Prausnitz, M. R., J. D. Corbet, J. A. Gimm, D. E. Golan, R. Langer, and J. C. Weaver. 1995. Millisecond measurement of transport during and after an electroporation pulse. *Biophys. J.* 98:1864–1870.

Rols, M. P., and J. Teissié. 1990. Electropermeabilization of mammalian cells: quantitative analysis of the phenomenon. *Biophys. J.* 58: 1089–1098.

Rossignol, D. P., G. L. Decker, W. J. Lennarz, T. Y. Tsong, and J. Teissié. 1983 Induction of calcium-dependent, localized cortical granule breakdown in sea-urchin eggs by voltage pulsation. *Biochim. Biophys. Acta*. 763:346–355.

Sator, V., M. A. Raftery, and M. Martinez-Carrion. 1977. Propidium as a probe of acetylcholine receptor binding sites. *Arch. Biochem. Biophys.* 184:95–102.

Schwister, K., and B. Deuticke. 1985. Formation and properties of aqueous leaks induced in human erythrocytes by electrical breakdown. *Biochim. Biophys. Acta*. 816:332–348.

Sixou, S., and J. Teissié. 1993. Exogenous uptake and release of molecules by electroloaded cells: a digitized videomicroscopy study. *Bioelectrochem. Bioenerg.* 31:237–257.

Teissié, J., and M. P. Rols. 1993. An experimental evaluation of the critical potential difference inducing cell membrane electropermeabilization. *Biophys. J.* 65:409–413.

Teissié, J., and T. Y. Tsong. 1980. Evidence of voltage-induced channel opening in Na/K ATPase of human erythrocyte membrane. *J. Membr. Biol.* 55:133–140.

Teissié, J., and T. Y. Tsong. 1981. Electric field induced transient pores in phospholipid bilayer vesicles. *Biochemistry*. 20:1548–1554.

Tekle, E., R. D. Astumian, and P. B. Chock. 1990. Electro-permeabilization of cell membrane: effect of the resting membrane potential. *Biochem. Biophys. Res. Commun.* 172:282–287.

Tekle, E., R. D. Astumian, and P. B. Chock. 1994. Selective and asymmetric molecular transport across electroporated cell membranes. *Proc. Natl. Acad. Sci. U.S.A.* 91:11512–11516.

Teruel, M. N., and T. Meyer. 1997. Electropation-induced formation of individual calcium entry sites in the cell body and processes of adherent cells. *Biophys. J.* 73:1785–1796.

Tovar, O., and L. Tung. 1992. Electroporation and recovery of cardiac cell membrane with rectangular voltage pulses. *Am. J. Physiol*. 263: H1128–H1136.

Tsong, T. Y. 1991. Electroporation of cell membranes. *Biophys. J.* 60: 297–306.

Van Dinten, L. C., J. A. Den Boon, A. L. Wassenaar, W. J. Spaan, and E. J. Snijder. 1997. An infectious arterivirus cDNA clone: identification of a replicase point mutation that abolishes discontinuous mRNA transcription. *Proc. Natl. Acad. Sci. U.S.A.* 94:991–996.

Verspohl, E. J, I. Kaiserling-Buddemeier, and A. Wienecke. 1997. Introducing specific antibodies into electropermeabilized cells is a valuable tool for eliminating specific cell functions. *Cell Biochem. Funct.* 15: 127–134.